

## Rotational diffusion tensor of nucleic acids from $^{13}\text{C}$ NMR relaxation

Jerome Boisbouvier<sup>a</sup>, Zhengrong Wu<sup>a</sup>, Arika Ono<sup>b</sup>, Masatsune Kainosho<sup>b</sup> & Ad Bax<sup>a,\*</sup>

<sup>a</sup>Laboratory of Chemical Physics, National Institute of Diabetes and Digestive and Kidney Diseases, National Institutes of Health, Bethesda, Maryland 20892-0520, U.S.A.; <sup>b</sup>CREST and Graduate School of Science, Tokyo Metropolitan University, 1-1 Minami-oshawa, Hachioji, Tokyo 192-0397, Japan

Received 19 February 2003; Accepted 5 May 2003

**Key words:** anisotropy,  $^{13}\text{C}$  relaxation, Dickerson dodecamer, diffusion anisotropy, nucleic acids, rotational diffusion

### Abstract

Rotational diffusion properties have been derived for the DNA dodecamer  $d(\text{CGCGAATTCGCG})_2$  from  $^{13}\text{C}$   $R_{1\rho}$  and  $R_1$  measurements on the  $\text{C}_{1'}$ ,  $\text{C}_{3'}$ , and  $\text{C}_{4'}$  carbons in samples uniformly enriched in  $^{13}\text{C}$ . The narrow range of C-H bond vector orientations relative to the DNA axis make the analysis particularly sensitive to small structural deviations. As a result, the  $R_{1\rho}/R_1$  ratios are found to fit poorly to the crystal structures of this dodecamer, but well to a recent solution NMR structure, determined in liquid crystalline media, even though globally the structures are quite similar. A fit of the  $R_{1\rho}/R_1$  ratios to the solution structure is optimal for an axially symmetric rotational diffusion model, with a diffusion anisotropy,  $D_{\parallel}/D_{\perp}$ , of  $2.1 \pm 0.4$ , and an overall rotational correlation time,  $(2D_{\parallel} + 4D_{\perp})^{-1}$ , of 3.35 ns at 35 °C in  $\text{D}_2\text{O}$ , in excellent agreement with values obtained from hydrodynamic modeling.

### Introduction

$^{15}\text{N}$  NMR relaxation rates are widely used to derive rotational diffusion properties of proteins (Kay et al., 1989; Barbato et al., 1992; Wagner, 1993; Hansen et al., 1994; Tjandra et al., 1995; Wand et al., 1996; Lee et al., 1997; Dosset et al., 2000). Knowledge of the rotational diffusion tensor is also a prerequisite for deriving accurate information on internal dynamics from heteronuclear relaxation rates (Schurr et al., 1994; Tjandra et al., 1996; Cordier et al., 1998). For proteins with a significantly anisotropic diffusion tensor, the autorelaxation rates can provide information on the orientation of bond vectors relative to the diffusion tensor, and therefore on the relative orientation of protein domains (Bruschweiler et al., 1995; Tjandra et al., 1997; Ghose et al., 2001; Ulmer et al., 2002).

Nucleic acids frequently have quite elongated structures, and determination of their full rotational diffusion tensor is therefore a prerequisite for the ac-

curate study of their internal dynamics. It has also been pointed out that ignoring the effects of rotational diffusion anisotropy can have serious consequences when interpreting interproton NOEs in terms of tight distance restraints (Withka et al., 1992). Other, more recently proposed experiments measure cross-correlated relaxation rates to determine the nucleic acid backbone conformation and the sugar pucker (Felli et al., 1999; Richter et al., 2000; Boisbouvier et al., 2000). However, besides the angle between the correlated interactions, the orientation of each individual interaction relative to the anisotropic rotational diffusion tensor also affects these relaxation rates.

Despite the increasing need for accurate knowledge of the hydrodynamic properties of nucleic acids in solution, few NMR attempts to determine overall rotational diffusion properties of nucleic acids have been reported to date (Akke et al., 1997; Kojima et al., 1998). There are several factors that make experimental determination of the diffusion tensor from NMR relaxation data more difficult for nucleic acids than for proteins. First,  $^{15}\text{N}$ - $\{^1\text{H}\}$  dipolar spin relax-

\*To whom correspondence should be addressed. E-mail: bax@nih.gov

ation rates, widely used for proteins, are limited to relatively few sites in nucleic acids, and in helical conformations, their orientational distribution relative to the helix axis tends to be very narrow.  $^{13}\text{C}$ - $^1\text{H}$  spin pairs are more abundant and cover a less narrow distribution, but quantitative measurement of the  $^{13}\text{C}$ - $\{^1\text{H}\}$  dipolar contribution to the  $^{13}\text{C}$  relaxation rates is complicated by the presence of  $^{13}\text{C}$ - $^{13}\text{C}$  dipolar interactions and  $^1J_{\text{CC}}$  couplings. In order to simplify spin systems into isolated  $^{13}\text{C}$ - $^1\text{H}$  pairs, natural abundance samples have been used (Borer et al., 1994; Spielmann, 1998). The use of fractionally  $^{13}\text{C}$ -labeled samples, in combination with selection of isolated  $^{13}\text{C}$  sites, was first used in proteins (Wand et al., 1996), and has also been applied to nucleic acids (Boisbouvier et al., 1999). Alternatively, site-specific  $^{13}\text{C}$  enrichment may be used (Paquet et al., 1996), or analysis can be restricted to the isolated  $^{13}\text{C}_2$ - $^1\text{H}_2$  in adenosine and  $^{13}\text{C}_8$ - $^1\text{H}_8$  in purine bases. Unfortunately, these aromatic sites have orientational distributions that are as poor as those of the imino  $^{15}\text{N}$ - $^1\text{H}$  vectors: For  $d(\text{CGCGAATTCGCG})_2$ , the angle between the helical axis and base C-H and N-H vectors equals  $4 \pm 4^\circ$  (Wu et al., 2003); for A-form RNA these angles are  $14 \pm 6^\circ$  (Klosterman et al., 1999). Moreover, the base  $^{13}\text{C}$ - $^1\text{H}$  pairs also have large chemical shift anisotropies (CSA) that are not collinear with their  $^{13}\text{C}$ - $^1\text{H}$  dipolar interactions, complicating analysis of their relaxation rates.

Standard methods are available to determine the orientation and magnitude of the rotational diffusion tensor from analysis of the  $R_2/R_1$  relaxation rate ratios, which, to a good approximation, are independent of rapid internal motions (Barbato et al., 1992; Brunschweiler et al., 1995; Lee et al., 1997; Dosset et al., 2000; Osborne and Wright, 2001). Methods for the accurate measurement of these rates in proteins have been described by Kay and coworkers (Yamazaki et al., 1994). The present study shows that accurate  $^{13}\text{C}$ -relaxation rates can be measured in uniformly  $^{13}\text{C}$ -labeled nucleic acids and that these are sufficient to determine the rotational diffusion tensor, a prerequisite to further analysis of internal dynamics and local conformation from auto- and cross-correlated relaxation rates. We focus on the relaxation rates of aliphatic sugar  $^{13}\text{C}$ - $^1\text{H}$  pairs, for which the carbon nuclei have much smaller CSA than base carbons. Measurements are demonstrated for the so-called Dickerson DNA dodecamer  $d(\text{CGCGAATTCGCG})_2$  (Wing et al., 1980), for which several high-resolution NMR structures have been determined recently (Tjandra et al., 2000;

Wu et al., 2003; pdb code 1NAJ). It is demonstrated that due to the limited number of  $^{13}\text{C}$  sites available and their non-uniform orientational distribution, high accuracy of the structure is a prerequisite for obtaining agreement between relaxation data and orientation of corresponding vectors in the structure. Considering that the global diffusion tensor can also be estimated accurately from hydrodynamic modeling, this suggests that these relaxation rates are useful for refining the structures of highly elongated nucleic acid structures, analogous to previous use of  $^{15}\text{N}$  relaxation rates for protein structure refinement (Tjandra et al., 1997; Ghose et al., 2001; Ulmer et al., 2002).

## Experimental section

All NMR experiments were carried out at  $35^\circ\text{C}$  on a Bruker DRX spectrometer operating at 600 MHz  $^1\text{H}$  frequency, equipped with a cryogenic, triple resonance probehead. Two different samples were used for these relaxation rates measurements:  $d(\text{CGCGAATTCGCG})_2$  and  $d(\text{CGCGAATTCGCG})_2$ , where bold-faced nucleotides are uniformly labeled with  $^{13}\text{C}$  and  $^{15}\text{N}$ , prepared as described elsewhere (Ono et al., 1998). Each sample contained 0.4 mM duplex, 50 mM KCl, 1 mM EDTA, and 10 mM potassium phosphate buffer (pH 7.0) in 99.9%  $\text{D}_2\text{O}$ , in a 250  $\mu\text{l}$  Shigemi microcell. The total experimental time for relaxation measurement for each sample was ca. 24 h. For the  $T_1$  measurements,  $^{13}\text{C}$  magnetization was alternately placed along  $+z$  and  $-z$  at the beginning of the relaxation period, and the two corresponding fids were subtracted, thereby converting the magnetization recovery curve to a simple exponential decay (Sklenar et al., 1987).  $T_1$  relaxation decay was sampled at 15 different time points (20, 40, 60, 80, 100, 120, 140, 200, 280, 360, 440, 520, 600, 680, 760 ms). Each  $T_{1\rho}$  relaxation curve was sampled with seven points (10, 20, 30, 40, 60, 80, 100 ms). Each recorded spectrum consisted of a  $125^* \times 512^*$  data matrix, corresponding to acquisition times of 25 ms ( $t_1$ ) and 64 ms ( $t_2$ ). Data were processed and analyzed with the NMRPipe software package (Delaglio et al., 1995).

## Theoretical section

In uniformly  $^{13}\text{C}$ -labeled nucleic acids, each sugar methine carbon (i.e.,  $\text{C}_{1'}$ ,  $\text{C}_{3'}$ ,  $\text{C}_{4'}$  for DNA and RNA, plus  $\text{C}_{2'}$  for RNA only) is covalently bound to either

one or two  $^{13}\text{C}$  spins. Those interacting spins can be either singly protonated (denoted  $C_i^1$ ) or doubly protonated (denoted  $C_j^2$ ;  $C_{5'}$  for DNA and RNA, and  $C_{2'}$  for DNA). In such spin systems, the time dependencies of the longitudinal (if measured as described in the Results section) and transverse magnetization of a given methine carbon are:

$$\frac{d(\Delta C_z(t))}{dt} = - \left( \rho^{\text{CH}} + \sum_i \rho^{\text{CC}_i^1} + \sum_j \rho^{\text{CC}_j^2} \right) \quad (1)$$

$$(\Delta C_z(t)) - \sum_i \sigma^{\text{CC}_i^1} (\Delta C_{iZ}^1(t)) - \sum_j \sigma^{\text{CC}_j^2} (\Delta C_{jZ}^2(t))$$

$$\frac{d(C_+(t))}{dt} = - \left( R_2^{\text{CH}} + \sum_i R_2^{\text{CC}_i^1} + \sum_j R_2^{\text{CC}_j^2} \right) \quad (2)$$

$$(C_+(t)),$$

where  $\Delta C_z(t)$  is the difference in longitudinal magnetization at time point  $t$ , when  $^{13}\text{C}$  magnetization is placed along the  $+z$  or  $-z$  axis at  $t = 0$ ;  $C_+(t)$  is the transverse magnetization during the  $R_{1\rho}$  experiment;  $\rho^{\text{CH}}$  and  $R_2^{\text{CH}}$  are the regular longitudinal and transverse relaxation rates for an isolated  $^{13}\text{C}$ - $^1\text{H}$  system;  $\rho^{\text{CC}}$ ,  $R_2^{\text{CC}}$ ,  $\sigma^{\text{CC}}$  represent longitudinal and transverse  $^{13}\text{C}$ - $^{13}\text{C}$  dipolar auto- and cross relaxation terms, respectively. These rates are given by:

$$\rho^{\text{CH}} = (\xi^{\text{CH}})^2 [3J^{\text{CH}}(\omega_C) + J^{\text{CH}}(\omega_H - \omega_C) + 6J^{\text{CH}}(\omega_H + \omega_C)] + \frac{2(\gamma_C \Delta\sigma B_0)^2}{15} J^{\text{CH}}(\omega_C) \quad (3)$$

$$\rho^{\text{CC}} = (\xi^{\text{CC}})^2 [J^{\text{CC}}(0) + 3J^{\text{CC}}(\omega_C) + 6J^{\text{CC}}(2\omega_C)] \quad (4)$$

$$\sigma^{\text{CC}} = (\xi^{\text{CC}})^2 [6J^{\text{CC}}(2\omega_C) - J^{\text{CC}}(0)] \quad (5)$$

$$R_2^{\text{CH}} = \frac{(\xi^{\text{CH}})^2}{2} [4J^{\text{CH}}(0) + 3J^{\text{CH}}(\omega_C) + J^{\text{CH}}(\omega_H - \omega_C) + 6J^{\text{CH}}(\omega_H) + 6J^{\text{CH}}(\omega_H + \omega_C)] + \frac{(\gamma_C \Delta\sigma B_0)^2}{45} [4J^{\text{CH}}(0) + 3J^{\text{CH}}(\omega_C)] \quad (6)$$

$$R_2^{\text{CC}} = \frac{(\xi^{\text{CC}})^2}{2} [5J^{\text{CC}}(0) + 9J^{\text{CC}}(\omega_C) + 6J^{\text{CC}}(2\omega_C)]. \quad (7)$$

Above,  $(\xi^{\text{IS}})^2 = [(\mu_0 \hbar \gamma_I \gamma_S) / (4\pi (r_{I-S}^3))]^2 / 10$ ,  $\Delta\sigma$  is the CSA of carbon C and  $J^{\text{PQ}}(\omega)$  is the spectral density

function which samples motion of the P-Q vector at frequency  $\omega$ . In Equation 7, the coefficients for  $J^{\text{CC}}(0)$  and  $J^{\text{CC}}(\omega_C)$  apply for the case where the spin-lock field is sufficiently weak that only the effective rf field for the spin type of interest is transverse. For strong spin lock fields, these coefficients increase from 5 to 9, and from 9 to 15, respectively (Ravikumar et al., 1991).

If  $p$ ,  $m$ , and  $n$  are the direction cosines of the P-Q vector relative to the  $x$ ,  $y$ , and  $z$  principal axes of the rotational diffusion tensor, respectively, the spectral density function for the general case of rigid body anisotropic reorientation is given by (Woessner, 1962):

$$J^{\text{XY}}(\omega) = \sum_{k=1, \dots, 5} A_k \tau_k / (1 + (\omega \tau_k)^2), \quad (8)$$

with  $A_1 = 6m^2n^2$ ,  $A_2 = 6p^2n^2$ ,  $A_3 = 6p^2m^2$ ,  $A_4 = d - e$ ,  $A_5 = d + e$ , where  $d = [3(p^4 + m^4 + n^4) - 1]/2$ ,  $e = [\delta_x(3p^4 + 6m^2n^2 - 1) + \delta_y(3m^4 + 6p^2n^2 - 1) + \delta_z(3n^4 + 6m^2p^2 - 1)]/6$ , and  $\delta_i = (D_i - D) / (D^2 - L^2)^{1/2}$ .  $D$  is defined as one third of the trace of the diffusion tensor,  $D = (D_{xx} + D_{yy} + D_{zz})/3$ , and  $L^2 = (D_{xx}D_{yy} + D_{xx}D_{zz} + D_{yy}D_{zz})/3$ . The corresponding time constants are defined as follows,  $\tau_1 = (4D_{xx} + D_{yy} + D_{zz})^{-1}$ ,  $\tau_2 = (4D_{yy} + D_{xx} + D_{zz})^{-1}$ ,  $\tau_3 = (4D_{zz} + D_{xx} + D_{yy})^{-1}$ ,  $\tau_4 = [6(D + (D^2 - L^2)^{1/2})]^{-1}$ ,  $\tau_5 = [6(D - (D^2 - L^2)^{1/2})]^{-1}$ . Strictly speaking, specific spectral densities should be introduced because  $^{13}\text{C}$  CSA tensors in sugars are generally not collinear with the  $^{13}\text{C}$ - $^1\text{H}$  bond vector, and vary with sugar puckering (Dejaegere and Case, 1998; Boisbouvier et al., 2000). However, the  $^{13}\text{C}$  sugar CSA is generally small (an average value of  $\Delta\sigma = 40$  ppm was used for the CSA of all sugar carbons), and at 14.1 T, the CSA interaction accounts for less than 3% of the total relaxation. Therefore, our assumption of collinear CSA and  $^{13}\text{C}$ - $^1\text{H}$  dipolar interactions results in negligible errors.

Considering the interatomic distances ( $r_{\text{C-H}} = 1.09 \text{ \AA}$  and  $r_{\text{C-C}} = 1.52 \text{ \AA}$ ) and gyromagnetic ratios, it is clear that the  $^{13}\text{C}$ - $^{13}\text{C}$  contribution to  $R_2$  (Equation 7) can be safely ignored relative to the  $^1\text{H}$ - $^{13}\text{C}$  contribution (Equation 6). Therefore the transverse relaxation rate measured in a uniformly  $^{13}\text{C}$  enriched sugar is similar to the rate expected for an isolated  $^{13}\text{C}$ - $^1\text{H}$  two-spin system undergoing the same motion. Comparison of Equations 3, 4 and 5 indicates that  $\rho^{\text{CC}} + \sigma^{\text{CC}} \ll \rho^{\text{CH}}$ . If the repetition rate between scans is sufficiently slow, comparable amounts of initial magnetization are available for the different  $^{13}\text{C}$  sites at the start of the  $T_1$  relaxation recovery delay.

In this case, the  $^{13}\text{C}$ - $^{13}\text{C}$  dipolar contribution from the neighboring methine carbons,  $\text{C}^1$ , to the auto- and cross relaxation rates of the studied carbon  $\text{C}$  largely cancel, provided  $R_1$  is derived from the initial slope of the relaxation decay curve. Note that the remaining  $^{13}\text{C}$ - $^{13}\text{C}$  dipolar terms,  $J^{\text{CC}}(\omega_{\text{C}})$  and  $J^{\text{CC}}(2\omega_{\text{C}})$ , contribute less than 2% to the  $R_1$  rates, and may therefore safely be neglected. The duration of the refocused INEPT element used to transfer proton magnetization to in-phase carbon magnetization is adjusted such that transfer to  $\text{CH}_2$  and  $\text{CH}_3$  groups is minimized, whereas methine sites are near their maximum. Therefore the last term of Equation 1, corresponding to the cross-relaxation of the studied carbon  $\text{C}$  with its methylene neighbor, can also be ignored. For  $\text{C}_{1'}$ ,  $\text{C}_{3'}$  and  $\text{C}_{4'}$  nuclei in uniformly  $^{13}\text{C}$  labeled DNA, which each have one  $\text{CH}_2$  and none or one  $\text{CH}$  group as neighbors, the longitudinal relaxation rate extracted from a mono-exponential fit to the initial decay can be approximated by:

$$R_1 = (\rho^{\text{CH}} + \rho^{\text{CC}_j^2}). \quad (9)$$

Note that for  $\text{C}_{1'}$ ,  $\text{C}_{2'}$ , and  $\text{C}_{3'}$  in RNA, the extracted  $R_1$  does not contain any  $^{13}\text{C}$ - $^{13}\text{C}$  dipolar contribution, as they are adjacent to methine sites only.

## Results and Discussion

For uniformly  $^{13}\text{C}$ -labelled biomolecules, use of the common Carr–Purcell–Meiboom–Gill sequence for measuring the transverse relaxation rates leads to echo-modulation during the  $^{13}\text{C}$  relaxation delay, caused by the large  $^1J_{\text{CC}}$  coupling (ca. 40 Hz in sugars). However, it has been shown that use of a low-power spin lock field during the relaxation decay period yields reliable relaxation rates in uniformly labeled proteins (Yamazaki et al., 1994). During such spin lock periods, it is important that homonuclear Hartmann-Hahn magnetization transfer is minimized by ensuring that the difference in effective field strengths for two coupled spins is sufficiently large (Bax and Davis, 1985):

$$\Delta\nu_{\text{eff}} = |\nu_{1,\text{eff}} - \nu_{2,\text{eff}}| \gg ^1J_{\text{CC}}, \quad (10)$$

where  $\nu_{a,\text{eff}} = (\nu^2 + \delta_a^2)^{1/2}$ , with  $\nu$  the radiofrequency (rf) field strength in Hertz, and  $\delta_a$  the resonance offset of nucleus  $a$ , also in Hertz.

For application to the DNA oligomer, two series of  $R_{1\rho}$  experiments were recorded, both with a  $^{13}\text{C}$

spin-lock field strength of 2 kHz, with the  $^{13}\text{C}$  carrier positioned either at the center of the  $\text{C}_{3'}$  resonances (78 ppm) or near the middle of  $\text{C}_{1'}$  and  $\text{C}_{4'}$  spectral region (86 ppm). Each type of sugar carbon resonates in a distinct spectral region, thereby enabling the  $R_{1\rho}$  values to be measured without interference from homonuclear Hartmann-Hahn magnetization transfer. The closest resonances occur for  $\text{C}_{4'}$  and  $\text{C}_{3'}$  ( $\Delta\delta \approx 8$  ppm). At 14.1 T, with the spin-lock strength used, we have in this particular case  $\Delta\nu_{\text{eff}} \approx 300$  Hz, which meets the requirement of Equation 10. Note that for application to RNA,  $R_{1\rho}$  measurement for  $\text{C}_{2'}$  and  $\text{C}_{3'}$  resonances may be complicated by the proximity of their resonances, and it may be advantageous to position the carrier to one side of the  $\text{C}_{2'}/\text{C}_{3'}$  region. Owing to the generally non-zero value of the  $^{13}\text{C}$  offset,  $\delta$ , the measured relaxation rate,  $R_{1\rho}^{\text{meas}}$ , is an admixture of  $R_{1\rho}$  and  $R_1$  (Akke and Palmer, 1996):

$$R_{1\rho}^{\text{meas}} = R_1 \cos^2 \theta + R_{1\rho} \sin^2 \theta \quad (11)$$

with  $\theta = \tan^{-1}(\nu/\delta)$ . Equation 11 was used to extract the true ( $R_{1\rho}$ ,  $R_1$ ) values from  $R_{1\rho}^{\text{meas}}$  and  $R_1$ , which were obtained using standard experiments (Peng and Wagner, 1992). Briefly, the in-phase carbon magnetization after a refocused INEPT transfer is allowed to relax for a variable period, followed by frequency editing during a 25 ms constant-time evolution period. After this, the signal is transferred to  $^1\text{H}$  for detection. A single  $180^\circ$   $^1\text{H}$  pulse is applied at the mid-point of the  $^{13}\text{C}$  relaxation period to suppress cross-relaxation and CSA-dipole cross-correlated relaxation (Korzhnev et al., 2002), and  $^{13}\text{C}$  rf irradiation, off-resonance by 50 kHz, is applied during a fraction of the interscan-delay, in order to ensure that the same amount of total rf heating per scan is generated when varying the spin lock duration during  $R_{1\rho}$  measurements (Wang and Bax, 1993). Selectivity of the excitation of methine carbons during the  $R_1$  measurement was ensured by application of a selective  $^{13}\text{C}$   $180^\circ$  IBURP-shaped pulse (2-ms duration at 151 MHz  $^{13}\text{C}$  frequency, for a 14 ppm bandwidth inversion) (Geen and Freeman, 1991) in the first INEPT transfer.

Examples of  $R_1$  relaxation decay curves for  $\text{C}_{1'}$ ,  $\text{C}_{3'}$  and  $\text{C}_{4'}$  are presented in Figure 1. The initial decays fit well to mono-exponential functions (Figure 1A), which confirms that the contribution from the cross-relaxation terms in Equation 1 is negligible. Interestingly, the points sampled at longer relaxation delays (0.2–0.76 s) also fall on the curves fitted to the first seven points (0.02–0.14 s) (Figure 1A), indicating that even at longer decay times the effect of  $^{13}\text{C}$ - $^{13}\text{C}$

Table 1. Experimental relaxation rates and derived dynamic parameters<sup>a</sup>

Nucleus	Nucleotide	$R_{1\rho}$ (Hz) <sup>a</sup>	$R_1$ (Hz) <sup>b</sup>	$R_2/R_1$	$S^2$ <sup>c</sup>	$\tau_f$ (ps) <sup>c</sup>
C <sub>1'</sub>	1	7.1 ± 0.2	1.61 ± 0.01	4.40	0.40	52
	3	<i>11.3 ± 0.1<sup>a</sup></i>	<i>1.91 ± 0.02</i>	<i>5.91</i>	<i>0.73</i>	<i>10</i>
	4	<i>13.2 ± 0.2</i>	<i>2.08 ± 0.02</i>	<i>6.33</i>	<i>0.84</i>	–
	5	<i>13.1 ± 0.2</i>	<i>2.07 ± 0.02</i>	<i>6.36</i>	<i>0.83</i>	–
	7	<i>12.8 ± 0.2</i>	<i>1.96 ± 0.02</i>	<i>6.55</i>	<i>0.80</i>	–
	8	<i>13.0 ± 0.2</i>	<i>1.98 ± 0.02</i>	<i>6.56</i>	<i>0.81</i>	–
	9	<i>10.5 ± 0.1</i>	<i>2.01 ± 0.01</i>	<i>5.23</i>	<i>0.67</i>	43
	11	<i>10.7 ± 0.1</i>	<i>1.93 ± 0.01</i>	<i>5.54</i>	<i>0.69</i>	26
C <sub>3'</sub>	1	6.1 ± 0.1	1.48 ± 0.01	4.14	0.33	51
	4	<i>12.9 ± 0.2</i>	<i>2.02 ± 0.02</i>	<i>6.39</i>	<i>0.82</i>	–
	5	<i>13.1 ± 0.2</i>	<i>1.99 ± 0.02</i>	<i>6.59</i>	<i>0.82</i>	–
	6	<i>13.3 ± 0.2</i>	<i>2.01 ± 0.02</i>	<i>6.63</i>	<i>0.83</i>	–
	7	<i>12.3 ± 0.2</i>	<i>1.89 ± 0.01</i>	<i>6.50</i>	<i>0.77</i>	–
	8	<i>12.7 ± 0.3</i>	<i>1.91 ± 0.02</i>	<i>6.65</i>	<i>0.79</i>	–
	9	<i>10.5 ± 0.1</i>	<i>1.83 ± 0.01</i>	<i>5.72</i>	<i>0.67</i>	20
	C <sub>4'</sub>	1	8.15 ± 0.1	1.56 ± 0.01	5.23	0.45
4		<i>12.2 ± 0.1</i>	<i>1.95 ± 0.01</i>	<i>6.25</i>	<i>0.77</i>	17
5		<i>13.3 ± 0.2</i>	<i>1.85 ± 0.01</i>	<i>7.19</i>	<i>0.80</i>	–
6		<i>13.5 ± 0.3</i>	<i>1.86 ± 0.01</i>	<i>7.27</i>	<i>0.81</i>	–
7		<i>13.3 ± 0.2</i>	<i>1.88 ± 0.01</i>	<i>7.05</i>	<i>0.81</i>	–
8		<i>13.1 ± 0.2</i>	<i>1.95 ± 0.02</i>	<i>6.74</i>	<i>0.79</i>	24
9		<i>11.8 ± 0.1</i>	<i>1.95 ± 0.01</i>	<i>6.06</i>	<i>0.73</i>	30
12		<i>9.4 ± 0.1</i>	<i>1.89 ± 0.01</i>	<i>4.99</i>	<i>0.58</i>	57

<sup>a</sup>Italicized values correspond to the 19  $R_2/R_1$  ratios that were used to fit diffusion tensor, selected using the cut-off criterion of (Tjandra et al., 1996).  $R_{1\rho}$  values have been corrected for offset using Equation 11.

<sup>b</sup>Fits to all 15 experimental points (0.02–0.76 s).

<sup>c</sup> $S^2$  and  $\tau_f$  values were determined from the  $R_2$  and  $R_1$  values using the optimized axially symmetric model values as fixed parameters.

cross-relaxation remains negligible. This results from the fact that for small nucleic acids ( $\tau_c < 4$  ns) the contribution of carbon-carbon dipolar interaction to the relaxation is small compared to the proton-carbon interaction ( $\rho^{CC}/\rho^{CH} < 0.05$ ). However, for larger oligomers the  $^{13}\text{C}$ - $^{13}\text{C}$  contribution becomes more significant ( $\rho^{CC}/\rho^{CH} = 0.26$  for  $\tau_c = 10$  ns), and significant deviations from mono-exponential decay may occur. Mono-exponential decay, free of  $^{13}\text{C}$ - $^{13}\text{C}$  echo modulation, is also observed for the  $R_{1\rho}$  experiments (Figure 1B), permitting accurate measurement of the transverse relaxation rates.

Due to the similarity in sequence (CGCG) at the 3' and 5' ends of the d(CGCGAATTCGCG)<sub>2</sub> sequence of the Dickerson dodecamer, extensive overlap oc-

curs between  $^{13}\text{C}$ - $^1\text{H}$  correlations of G2 and G10 and also between C3 and C11 (Tjandra et al., 2000). Altogether, only 24 out of the potential 36  $^{13}\text{C}$ - $^1\text{H}$  correlations were sufficiently well resolved to permit accurate measurement of the relaxation rates (Table 1). In the absence of significant fast internal mobility or conformational exchange, the  $R_2/R_1$  ratio should depend only on the global reorientation of the nucleic acids, permitting extraction of the diffusion tensor. Therefore, it is important to exclude from the fit the C-H vectors displaying such internal motion. C-H vectors of 5' and 3' terminal nucleotides (C1 and G12) have been excluded as they are undergoing fast internal motion. Based on statistical criteria proposed by Tjandra et al. (1996), none of the remaining 19

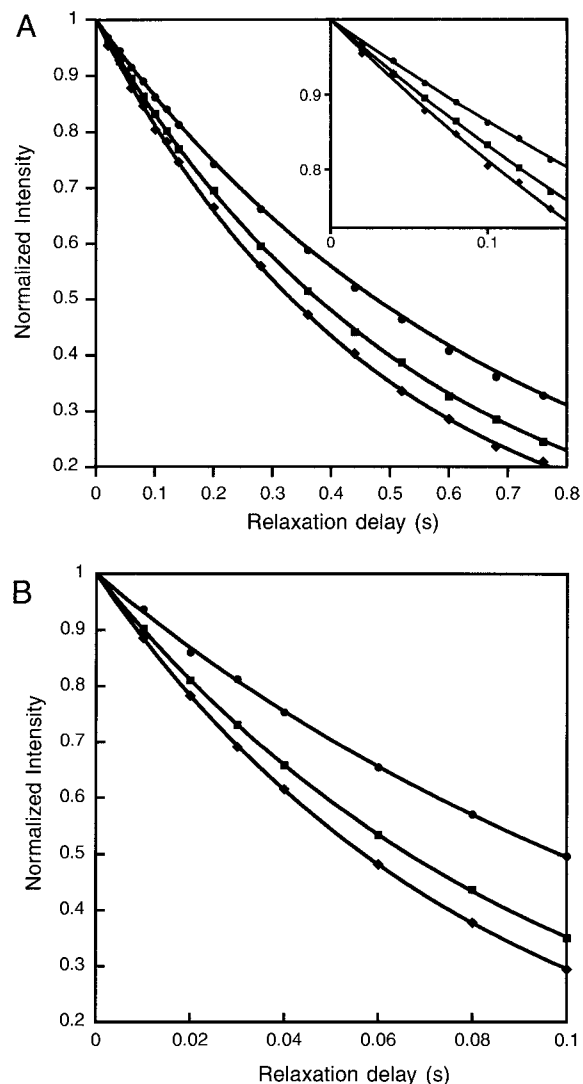


**Figure 1.** Example of (A)  $R_1$  and (B)  $R_{1\rho}$  relaxation decay curves. A.  $R_1$  relaxation decay was sampled at 15 different time points (20, 40, 60, 80, 100, 120, 140, 200, 280, 360, 440, 520, 600, 680, 760 ms), but the curves shown are exponential fits to the first seven points only. (■), (●) and (◆) correspond to the experimental points for  $C_{4'}$  of A(5),  $C_{3'}$  of C(1) and  $C_{1'}$  of G(4), respectively. The first 150 ms of the relaxation decays are expanded in the top right corner of panel A. Each  $T_{1\rho}$  relaxation curve (B) was sampled with seven points (10, 20, 30, 40, 60, 80, 100 ms), and the optimized exponential fits are represented by solid lines. (■), (●) and (◆) correspond to the experimental points for  $C_{3'}$  of C(9),  $C_{1'}$  of C(1) and  $C_{4'}$  of G(4), respectively.

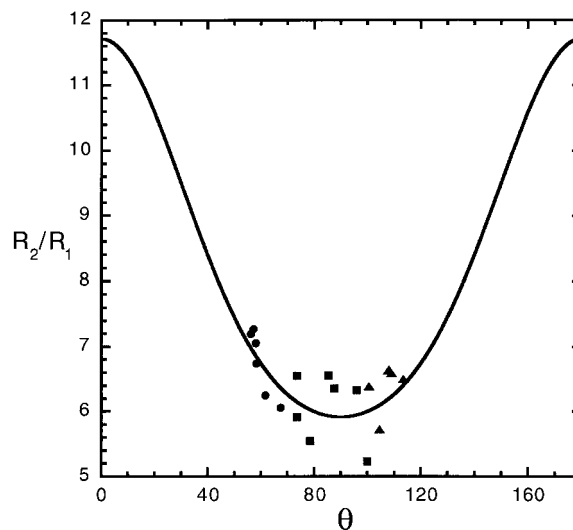


**Figure 2.** Plot of the  $^{13}\text{C}$   $R_2/R_1$  ratios observed at 14.1 T versus the angle  $\theta$  between CH bond vectors and the unique axis of the inertia tensor. (■), (●) and (◆) correspond to the experimental points for  $C_{1'}$ ,  $C_{3'}$  and  $C_{4'}$  respectively. The angles have been extracted from the liquid crystal structure (PDB code 1NAJ). The solid line corresponds to the theoretical dependence of  $R_2/R_1$  on  $\theta$  calculated for the best fit axially symmetric diffusion tensor model ( $\tau_c = 3.35$  ns,  $D_{\parallel}/D_{\perp} = 2.1$ ,  $\theta = 3^\circ$ ,  $\phi = -90^\circ$ ). The standard deviation between experimental and calculated values is 0.39.

C–H vectors displays conformational exchange that significantly affects the  $R_1/R_{1\rho}$  ratio.

These 19 remaining data points are used for defining the diffusion tensor. However, due to the palindromic nature of the oligomer, these 19 values actually correspond to 38 sites in the oligomer. The distribution of the  $R_2/R_1$  ratios measured for these sites is shown in Figure 2. Unfortunately, the above C–H vectors have a fairly narrow orientational distribution and only sample angles between  $0^\circ$  to  $35^\circ$  from the plane perpendicular to the helix axis. Nevertheless, the 25% variation observed in the  $R_2/R_1$  ratio, which considerably exceeds the estimated experimental error in this ratio ( $\pm 3\%$ ), indicates that the anisotropy of the diffusion tensor is substantial.

In order to determine the orientation and magnitude of the principal components of the rotational diffusion tensor, we conduct a systematic grid search followed by Powell optimization to find the best agreement between experimental  $R_2/R_1$  ratios and values calculated using Equation 6 and 9. The diffusion parameters are obtained by minimizing the difference between measured and calculated ratios:

$$\xi^2 = \sum_{i=1}^N \left[ \frac{(R_2^{\text{meas}}/R_1^{\text{meas}} - R_2^{\text{calc}}/R_1^{\text{calc}})_i}{\sigma_i} \right]^2, \quad (12)$$

where  $\sigma_i$  equals the estimated error in the  $R_2^{\text{meas}}/R_1^{\text{meas}}$  ratio, and the superscripts ‘meas’ and ‘calc’ refer to the measured rates, and to the rates calculated for a given rotational diffusion model, assuming the time scale for internal motions,  $\tau_f$ , approaches zero. For  $^{15}\text{N}$  relaxation studies in proteins, the approximation that the  $R_2/R_1$  ratio is independent of rapid internal motions is widely used (Kay et al., 1989). For  $^{13}\text{C}$  relaxation studies in anisotropically diffusing nucleic acids, the situation is more complex and, strictly speaking, specific order parameters,  $\mathbf{S}^{2,\text{CH}}$ ,  $\mathbf{S}^{2,\text{CC}}$ , and  $\mathbf{S}^{2,\text{CSA}}$ , need to be introduced for the respective interactions. However, considering that for the deoxyribose carbons the CSA and  $^{13}\text{C}$ - $^{13}\text{C}$  dipolar interactions account for less than 5% of the total relaxation in the d(CGCGAATTCGCG)<sub>2</sub> dodecamer, the use of a single  $\mathbf{S}^2$  value for these three relaxation mechanisms results in negligible errors, and the approximation that the  $R_2/R_1$  ratio is independent of rapid internal motions remains valid.

During minimization of Equation 12, the experimental error for each  $R_1$  and  $R_{1\rho}$  rate has been set to 2%. An axially symmetric rotational diffusion model, with four variable parameters ( $\tau_c = [2\text{Tr}(\mathbf{D})]^{-1}$ ;  $D_{\parallel}/D_{\perp} = [2D_z/(D_x + D_y)]$ , and the angles  $\theta$  and  $\phi$  describing the orientation of its unique axis, yields a large improvement in the quality of the fit (Table 2). The  $\chi^2/N$  value drops from 9.01 to 5.09 when comparing the isotropic model with an axially symmetric model obtained by using the high-resolution structure of dodecamer solved in liquid crystalline medium (Wu et al., 2003) as reference. Because the fit between a model and experimental data generally improves with the number of adjustable parameters in the model function, the F-test (Bevington and Robinson, 1992) may be used to determine the statistical significance of the decrease in  $\chi^2$ . The computed probability,  $p$ , that the decrease in  $\chi^2/N$  value is obtained by chance, while adding three parameters to the fit, is 3%. For comparison, the introduction of two additional parameters, by using a fully asymmetric model (Table 2), does not yield a statistically significant improvement of the target function ( $p = 90\%$ ). An independent estimate of the rhombicity of the diffusion tensor can be obtained from the dodecamer’s inertia tensor. The ratios of the dodecamer’s three principal moments of inertia,  $I_{xx}/I_{yy}/I_{zz}$ , are 1.00/0.97/0.31, also indicating that rhombicity of the diffusion tensor is expected to

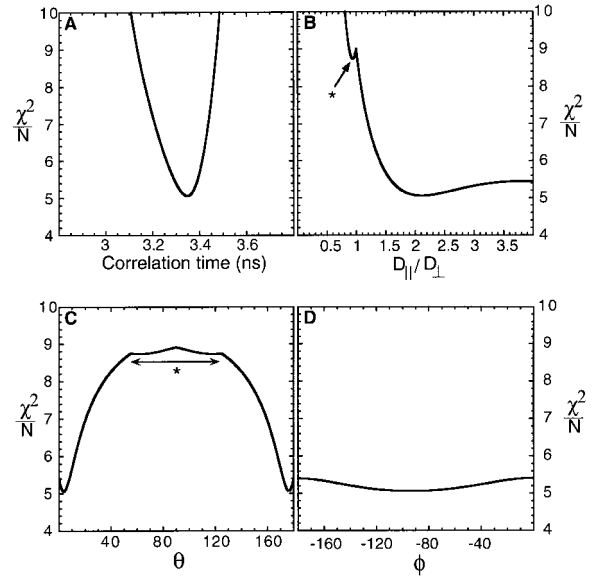


Figure 3. Cross sections through the four-dimensional  $\chi^2/N$  surface, at the position of the global minimum. (A)  $\chi^2/N$  as a function of  $\tau_c$ ; (B)  $\chi^2/N$  as a function of  $D_{\parallel}/D_{\perp}$ ; (C)  $\chi^2/N$  as a function of  $\theta$ ; (D)  $\chi^2/N$  as a function of  $\phi$ . These graphs were constructed by stepwise incrementing the independent variable ( $x$  axis), while for each such step adjusting the remaining three variables such that a minimum  $\chi^2/N$  is reached, using iterative minimization. Asterisks mark the oblate model.

be negligible. So for further analysis, only the statistically significant axially symmetric model will be considered.

The minimization of the difference between experimental and calculated  $R_2/R_1$  values (Figure 2), using Equation 12, converges to a defined prolate minimum (Figure 3) with a  $D_{\parallel}/D_{\perp}$  value of  $2.1 \pm 0.4$ , and an orientation of the unique principal axis which does not significantly differ from the corresponding principal axis of the inertia tensor (Figure 4). Taking into account the low angular dispersion of the C-H vectors (Figure 2), the orientation ( $\theta$ ) of the principal axis is well defined (Table 2). Note that the weak dependence of  $\chi^2$  on the  $\phi$  angle is a direct consequence of the small  $\theta$  value. When using an axially symmetric approximation, one oblate and one prolate minimum generally may be expected (Blackledge et al., 1998). For the Dickerson dodecamer, the oblate local minimum corresponds to a significantly higher value of the target function (Figure 3) and does not correspond to a statistically significant improvement over the isotropic model ( $p = 0.92$ ), and clearly only the prolate model applies.

Table 2. Best-fit rotational diffusion parameters for different diffusion models and different input structures

Structure <sup>a</sup>	Model	$\tau_c^{b,e}$	$D_{\parallel}/D_{\perp}^c$	$D_y/D_x^c$	$(\theta, \phi, \iota)^{c,e}$	$\chi^2/N$	$m^d$
	Iso.	$3.14 \pm 0.04$				9.01	1
1NAJ <sup>f</sup>	Ax. Sym.	$3.35 \pm 0.03$	$2.1 \pm 0.4$		$3 \pm 2, -90 \pm 43$	5.09	4
1NAJ <sup>f</sup>	Asymm.	$3.35 \pm 0.03$	$2.1 \pm 0.5$	$1.04 \pm 0.06$	$3 \pm 2, -90 \pm 45, 1 \pm 55$	5.01	6
1DUF <sup>f</sup>	Ax. Sym.	$3.35 \pm 0.03$	$1.9 \pm 0.4$		$3 \pm 3, -99 \pm 47$	6.17	4
1BNA	Ax. Sym.	$3.30 \pm 0.03$	$1.6 \pm 0.2$		$12 \pm 4, -57 \pm 24$	6.24	4
355D	Ax. Sym.	$3.26 \pm 0.04$	$1.3 \pm 0.2$		$15 \pm 12, -118 \pm 41$	7.70	4
1NAJ <sup>g</sup>	Ax. Sym.	3.00	2.16				
1NAJ <sup>h</sup>	Ax. Sym.		2.26				

<sup>a</sup>Structures are indicated by their PDB accession code.

<sup>b</sup>Effective correlation time (ns), calculated from  $(2\text{Tr}(\mathbf{D}))^{-1}$ .

<sup>c</sup> $(\theta, \phi, \iota)$  describe Euler rotation angles, correlating an arbitrary vector  $y'$  in the diffusion tensor frame to its orientation in the inertia tensor:  $y' = \mathbf{R}(\theta, \phi, \iota)y$ .

<sup>d</sup>Number of variables used in the fit.

<sup>e</sup>Uncertainties are derived using simulated datasets with ideal, calculated  $R_2/R_1$  values, to which noise is added such that the  $\chi^2/N$  value is the same as in the experimental data set.

<sup>f</sup>Values averaged over the NMR ensemble of structures.

<sup>g</sup>Calculated using the hydrodynamical model developed by (Tirado and Garcadelatorre, 1980) with a radius of 9.75 Å and a length of 37.5 Å.

<sup>h</sup>Calculated using Torchia's empirical formula:  $D_{\parallel}/D_{\perp} = (I_{\perp}/I_{\parallel})^{1/\sqrt{2}}$ , where  $I_{\parallel}/I_{\perp}$  is the ratio of the principal components of the inertia tensor (Copie et al., 1998).

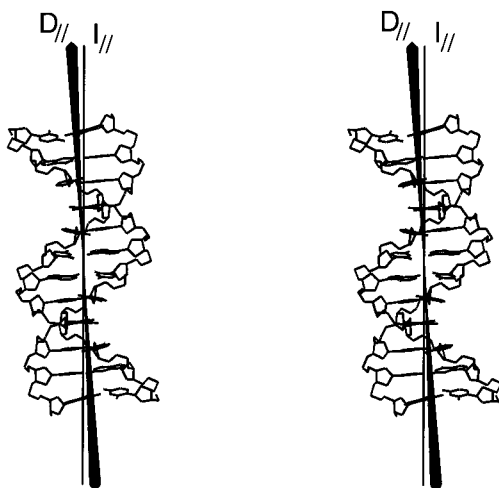


Figure 4. Stereo view of the orientations of the unique principal axes of the diffusion ( $D_{\parallel}$ ) and inertia ( $I_{\parallel}$ ) tensors relative to the dodecamer. The calculated uncertainty in the orientation of  $D_{\parallel}$  is represented by the width of the cone. Error analyses have been performed using simulated datasets with ideal, calculated  $R_2/R_1$  values, to which noise is added such that the  $\chi^2/N$  value is the same as in the experimental data set.

The hydrodynamic properties of the Dickerson dodecamer can also be predicted on the basis of its shape. For hydrodynamic calculations, the DNA dodecamer is well modeled as a cylinder with a radius of 9.75 Å and a length of 37.5 Å, as deter-

mined using the program Curves (Lavery and Sklenar, 1988). Using the hydrodynamic model developed by Tirado and Garcadelatorre (1980) for a cylindrically shaped molecule, the predicted values for  $\tau_c$  and  $D_{\parallel}/D_{\perp}$  ratio are 3.0 ns and 2.16, respectively, in good agreement with our experimental data. It is also interesting to note that the observed anisotropy agrees well with Torchia's empirical formula:  $D_{\parallel}/D_{\perp} = (I_{\perp}/I_{\parallel})^{1/\sqrt{2}} = 2.26$ , where  $I_{\parallel}/I_{\perp}$  is the ratio of the principal components of the inertia tensor (Copie et al., 1998).

Compared to the earlier liquid crystal NMR structure of the Dickerson dodecamer (Tjandra et al., 2000) (PDB code 1DUF), the new structure (1NAJ) fits considerably better (Table 2). This new structure has been refined against  $^{31}\text{P}$ - $^1\text{H}$  dipolar couplings (Wu et al., 2001b),  $^{31}\text{P}$  CSA effects (Wu et al., 2001a), quantitative  $^1\text{H}$ - $^1\text{H}$  dipolar couplings (Delaglio et al., 2001) and previously measured  $^1\text{H}$ - $^{13}\text{C}$  dipolar couplings. The two structures, 1DUF and 1NAJ, differ by a Cartesian coordinates rmsd of only 0.56 Å, which is mainly caused by a slight but systematic decrease in the helical rise (and thereby the total length) of the new structure. The root-mean-square difference in the orientations of the  $^{13}\text{C}$ - $^1\text{H}$  bond vectors in the two models is only 4.5°. Although best fitting of the  $R_2/R_1$  rates to the earlier NMR structure (1DUF) yields a diffu-

sion tensor with the same orientation and magnitude, the  $\chi^2/N$  value is more than 20% higher. For comparison, fits to two X-ray structures, PDB entries 1BNA (Dickerson and Drew, 1981) and 355D (Shui et al., 1998) are much poorer and consequently yield a diffusion anisotropy of lower magnitude (Zweckstetter and Bax, 2002). These results confirm that the previously observed differences between the crystalline and solution conformations of the dodecamer are not caused by the liquid crystalline medium. The orientations of the C-H vectors relative to the unique inertia principal axis differ by  $10.6 \pm 5.7^\circ$  between the X-Ray and the liquid crystalline structures (the structures differ by an atomic rmsd of 1.5 Å). As pointed out previously (Tjandra et al., 2000), these structural differences are mainly caused by a kink in the helix, induced by  $Mg^{2+}$  binding and intermolecular hydrogen bonds in the crystalline lattice. The much smaller differences in sugar C-H bond orientations between the two liquid crystal structures must be attributed to residual random errors in the two NMR structures.

### Concluding remarks

Our results indicate that accurate  $^{13}C$  transverse and longitudinal relaxation rates can be measured for sugar methines in uniformly  $^{13}C$  labeled nucleic acids. For the Dickerson DNA dodecamer investigated in this study, analysis of these relaxation parameters results in a rotational diffusion tensor that closely agrees with predictions based on hydrodynamic modeling. For extracting an accurate rotational diffusion tensor from experimental relaxation data for a B-form DNA helix, in which the sugar methine C-H vector distribution relative to its helical axis is rather small, it is particularly important that the structure and orientation of the C-H bond vectors is known at high accuracy. This requirement is underscored by our analyses of the relaxation data in terms of the different PDB structures. Even while the X-ray structures available for the Dickerson dodecamer are of high quality (structure 355D was solved at a resolution of 1.4 Å), and differs by only 0.5 Å from the newest solution NMR structure when considering the center six basepairs (which contribute 90% of the bond vectors used for determining the rotational diffusion tensor), our  $^{13}C$  relaxation data fit poorly to these X-ray structures (Table 2). The difference in bond vector orientations between a given structure and its true average in solution is sometimes referred to as structural noise. Analogous to what was

found for estimating alignment tensors from dipolar coupling data (Zweckstetter and Bax, 2002), structural noise on average will decrease the magnitude of the rotational diffusion anisotropy obtained when fitting  $R_1/R_2$  data to a given model. This is precisely what is observed for the Dickerson dodecamer when fitting the relaxation data to the X-ray structure and, to a lesser extent, to the earlier NMR structure.

Our study highlights the requirement for a very accurate solution structure when extracting the hydrodynamic properties of an oligonucleotide from NMR data, and the dipolar couplings measured in liquid crystalline medium appear an essential prerequisite for obtaining such structures. The difficulties encountered in previous attempts to study oligonucleotide hydrodynamic properties from  $^{13}C$  relaxation are likely caused by the absence of such dipolar data. On the flipside, our finding that for a highly refined structure good agreement is obtained between the experimental  $R_2/R_1$  ratios and ratios calculated for the corresponding orientations, relative to the modeled hydrodynamic diffusion tensor, indicates that these ratios may be used for structure refinement purposes.

### Acknowledgements

We thank David Bryce for useful suggestions, and Nico Tjandra and Shou-Lin Chang for providing us their relaxation analysis program, which has been modified to fit the dodecamer diffusion tensor to  $^{13}C$  relaxation rates. This work was supported by fellowship of Human Frontier Science Program (to JB).

### References

- Akke, M. and Palmer, A.G. (1996) *J. Am. Chem. Soc.*, **118**, 911–912.
- Akke, M., Fiala, R., Jiang, F., Patal, D. and Palmer, A.G.I. (1997) *RNA*, **3**, 702–709.
- Barbato, G., Ikura, M., Kay, L.E., Pastor, R.W. and Bax, A. (1992) *Biochemistry*, **31**, 5269–5278.
- Bax, A. and Davis, D.G. (1985) *J. Magn. Reson.*, **63**, 207–213.
- Bevington, P.R. and Robinson, D.K. (1992) *Data Reduction and Error Analysis for the Physical Sciences*, McGraw-Hill, New York.
- Blackledge, M., Cordier, F., Dosset, P. and Marion, D. (1998) *J. Am. Chem. Soc.*, **120**, 4538–4539.
- Boisbouvier, J., Brutscher, B., Pardi, A., Marion, D. and Simorre, J.P. (2000) *J. Am. Chem. Soc.*, **122**, 6779–6780.
- Boisbouvier, J., Brutscher, B., Simorre, J.P. and Marion, D. (1999) *J. Biomol. NMR*, **14**, 241–252.
- Borer, P.N., Laplante, S.R., Kumar, A., Zanatta, N., Martin, A., Hakkinen, A. and Levy, G.C. (1994) *Biochemistry*, **33**, 2441–2450.

- Bruschweiler, R., Liao, X.B. and Wright, P.E. (1995) *Science*, **268**, 886–889.
- Copie, V., Tomita, Y., Akiyama, S.K., Aota, S., Yamada, K.M., Venable, R.M., Pastor, R.W., Krueger, S. and Torchia, D.A. (1998) *J. Mol. Biol.*, **277**, 663–682.
- Cordier, F., Caffrey, M., Brutscher, B., Cusanovich, M.A., Marion, D. and Blackledge, M. (1998) *J. Mol. Biol.*, **281**, 341–361.
- Dejaegere, A.P., and Case, D.A. (1998) *J. Phys. Chem. A.*, **102**, 5280–5289.
- Delaglio, F., Grzesiek, S., Vuister, G.W., Zhu, G., Pfeifer, J. and Bax, A. (1995), *J. Biomol. NMR*, **6**, 277–293.
- Delaglio, F., Wu, Z.R. and Bax, A. (2001) *J. Magn. Reson.*, **149**, 276–281.
- Dickerson, R.E. and Drew, H.R. (1981) *J. Mol. Biol.*, **149**, 761–786.
- Dosset, P., Hus, J.C., Blackledge, M. and Marion, D. (2000) *J. Biomol. NMR*, **16**, 23–28.
- Felli, I.C., Richter, C., Griesinger, C. and Schwalbe, H. (1999) *J. Am. Chem. Soc.*, **121**, 1956–1957.
- Geen, H. and Freeman, R. (1991) *J. Magn. Reson.*, **93**, 93–141.
- Ghose, R., Fushman, D. and Cowburn, D. (2001) *J. Magn. Reson.*, **149**, 204–217.
- Hansen, A.P., Petros, A.M., Meadows, R.P. and Fesik, S.W. (1994) *Biochemistry*, **33**, 15418–15424.
- Kay, L.E., Torchia, D.A. and Bax, A. (1989) *Biochemistry*, **28**, 8972–8979.
- Klosterman, P.S., Shah, S.A. and Steitz, T.A. (1999) *Biochemistry*, **38**, 14784–14792.
- Kojima, C., Ono, A., Kainosho, M. and James, T.L. (1998) *J. Magn. Reson.*, **135**, 310–333.
- Korzhnev, D.M., Skrynnikov, N.R., Millet, O., Torchia, D.A. and Kay, L.E. (2002) *J. Am. Chem. Soc.*, **124**, 10743–10753.
- Lavery, R. and Sklenar, H. (1988) *J. Biomol. Struct. Dyn.*, **6**, 63–91.
- Lee, L.K., Rance, M., Chazin, W.I. and Palmer, A.G.I. (1997) *J. Biomol. NMR*, **9**, 287–298.
- Ono, A.M., Shiina, T., Ono, A. and Kainosho, M. (1998) *Tetrahedron Lett.*, **39**, 2793–2796.
- Osborne, M.J. and Wright, P.E. (2001) *J. Biomol. NMR*, **19**, 209–230.
- Paquet, F., Gaudin, F. and Lancelot, G. (1996) *J. Biomol. NMR*, **8**, 252–260.
- Peng, J.W. and Wagner, G. (1992) *J. Magn. Reson.*, **98**, 308–332.
- Ravikumar, M., Shukla, R. and Bothner-By, A.A. (1991) *J. Chem. Phys.*, **95**, 3092–3098.
- Richter, C., Reif, B., Griesinger, C. and Schwalbe, H. (2000) *J. Am. Chem. Soc.*, **122**, 12728–12781.
- Schurr, J.M., Babcock, H.P. and Fujimoto, B.S. (1994) *J. Magn. Reson. Ser. B*, **105**, 211–224.
- Shui, X.Q., McFail-Isom, L., Hu, G.G. and Williams, L.D. (1998) *Biochemistry*, **37**, 8341–8355.
- Sklenar, V., Torchia, D. and Bax, A. (1987) *J. Magn. Reson.*, **73**, 375–379.
- Spielmann, H.P. (1998) *Biochemistry*, **37**, 5426–5438.
- Tirado, M.M. and Garcia-delatorre, J. (1980) *J. Chem. Phys.*, **73**, 1986–1993.
- Tjandra, N., Feller, S.E., Pastor, R.W. and Bax, A. (1995) *J. Am. Chem. Soc.*, **117**, 12562–12566.
- Tjandra, N., Garrett, D.S., Gronenborn, A.M., Bax, A. and Clore, G.M. (1997) *Nat. Struct. Biol.*, **4**, 443–449.
- Tjandra, N., Tate, S., Ono, A., Kainosho, M. and Bax, A. (2000) *J. Am. Chem. Soc.*, **122**, 6190–6200.
- Tjandra, N., Wingfield, P., Stahl, S. and Bax, A. (1996) *J. Biomol. NMR*, **8**, 273–284.
- Ulmer, T.S., Werner, J.M. and Campbell, I.D. (2002) *Structure*, **10**, 901–911.
- Wagner, G. (1993) *Curr. Opin. Struct. Biol.*, **3**, 748–754.
- Wand, A.J., Urbauer, J.L., McEvoy, R.P. and Bieber, R.J. (1996) *Biochemistry*, **35**, 6116–6125.
- Wang, A.C. and Bax, A. (1993) *J. Biomol. NMR*, **3**, 715–720.
- Wing, R., Drew, H., Takano, T., Broka, C., Tanaka, S., Itakura, K. and Dickerson, R.E. (1980) *Nature*, **287**, 755–758.
- Withka, J.M., Swaminathan, S., Srinivasan, J., Beveridge, D.L. and Bolton, P.H. (1992) *Science*, **255**, 597–599.
- Woessner, D.E. (1962) *J. Chem. Phys.*, **37**, 647–654.
- Wu, Z.R., Delaglio, F., Tjandra, N., Zhurkin, V.B. and Bax, A. (2003) *J. Biomol. NMR*, **26**, 297–315.
- Wu, Z.R., Tjandra, N. and Bax, A. (2001a) *J. Am. Chem. Soc.*, **123**, 3617–3618.
- Wu, Z.R., Tjandra, N. and Bax, A. (2001b) *J. Biomol. NMR*, **19**, 367–370.
- Yamazaki, T., Muhandiram, R. and Kay, L.E. (1994) *J. Am. Chem. Soc.*, **116**, 8266–8278.
- Zweckstetter, M. and Bax, A. (2002) *J. Biomol. NMR*, **23**, 127–137.